Environmental Research 248 (2024) 118247

Contents lists available at ScienceDirect

Environmental Research

journal homepage: www.elsevier.com/locate/envres

Optimizing filters of activated carbons obtained from biomass residues for ethylene removal in agro-food industry devices

Ana M. Regadera-Macías, Sergio Morales-Torres, Luisa M. Pastrana-Martínez *, Francisco J. Maldonado-Hódar

NanoTech – Nanomaterials and Sustainable Chemicals Technologies, Department of Inorganic Chemistry, Faculty of Science, University of Granada, Avda. Fuente Nueva, s/n, ES18071, Granada, Spain

ARTICLE INFO

Keywords:
Ethylene
Olive stones
Porous carbon
Adsorption
Physical or chemical activation

ABSTRACT

A series of adsorbents (activated carbons, ACs) were synthesized by physical and chemical activation of olive stones (OS) and their textural and chemical characteristics determined by complementary techniques such as N_2 and CO_2 physisorption, pH of the point zero of charge (pH_{PZC}), HRSEM or XPS. Samples with a wide range of physicochemical properties were obtained by fitting the activation procedure. The performance of these adsorbents in filters working under dynamic conditions was studied by determining the corresponding breakthrough curves for the ethylene removal. The physicochemical transformations of OS during activation were related with the adsorptive performance of derivative ACs. Results were compared to those obtained using commercial carbons, in particular ACs, carbon black or carbon fibers, in order to identify the properties of these materials on influencing the adsorptive performance. In general, ACs from OS perform better than the commercial samples, being also easily regenerated and properly used during consecutive adsorption cycles. CO_2-activation showed to be the best synthesis option, leading to granular ACs with a suitable microporosity and surface chemistry. These results could favour the integration of this type of inexpensive materials on devices for the preservation of climacteric fruits, in a clear example of circular economy by reusing the agricultural residues.

1. Introduction

The development of porous materials to be used as effective adsorbents for the removal of pollutants (CO_2, Hg, volatile organic compounds (VOCs), acid gases, SO_x, NO_x, etc.) (Hsieh et al., 2021; Plata-Gryl et al., 2022; Yang et al., 2021) or molecular sieves for the concentration/separation/purification of gaseous mixtures (CO_2/CH_4, C_2H_6/C_2H_4, etc) (Cho et al., 2022; Hamyali et al., 2022) is a key aspect in many industrial or environmental processes. Specifically, the development of effective tools to control the atmosphere surrounding climacteric fruits during their storage or transport is a main task for the agro-food industry.

Refrigerated chambers used for storage or transport operate under controlled atmosphere with a fitted concentration of O_2, CO_2 or humidity. In addition, different VOCs emitted by the stored fruits are strictly limited to increase the durability of the fruit (Wei et al., 2021). Among them, ethylene (C_2H_4) acts as a ripening natural hormone being highly active even at very low concentrations (mg L^{-1}) (Keller et al., 2013), causing the senescence and discard of part of the stored fruits with the consequent economic loss. The ethylene removal from the atmosphere of these devices is therefore a target objective to reach the proper functioning.

Different technologies have been developed to delay fruit ripening such as the use of 1-methylcyclopropene (1-MCP) inhibiting the ethylene perception, potassium permanganate ($KMnO_4$) as scavenging agent, thermal/photo-catalysis and adsorption processes, and so on (Keller et al., 2013). Adsorption is traditionally used to remove organic compounds from aqueous or gaseous effluents. Despite the huge impact that research on new nanostructured materials (Metalorganic frameworks, zeolites, graphenes, etc.) is having on the development of specific adsorbents (Altintas and Keskin, 2022; Cho et al., 2022; Coros et al., 2020; de Menezes et al., 2022; Vivo-Vilches et al., 2015), the use of activated carbons (ACs) for such applications still occupies an important position (Vivo-Vilches et al., 2015). Different and abundant agro-wastes are available around the world, which can be valorised by transformation in advanced materials and integrated in the agro-food chain,

* Corresponding author.
E-mail address: lpastrana@ugr.es (L.M. Pastrana-Martínez).

https://doi.org/10.1016/j.envres.2024.118247
Received 14 November 2023; Received in revised form 29 December 2023; Accepted 17 January 2024
Available online 20 January 2024

e.g. for the removal of volatile organic compounds (VOCs) like ethylene, decreasing the carbon footprint according to the circular economy concept. Numerous and recent publications continue progressively trying to update these classic materials in different applications (Hamyali et al., 2022; Malini et al., 2023; Wu et al., 2020; Yang et al., 2021).

The physicochemical properties influencing on the adsorption process of ACs are related with their porous texture, surface area and chemical surface. These parameters can be adjusted by activation or functionalization treatments, but the transformations induced are highly dependent on the precursor and the experimental synthesis conditions used in each case. ACs can be prepared using very diverse cheap precursors such as industrial wastes, sewage sludge, mineral coals, polymers (spent tyres), etc., (Jones et al., 2021; Luján-Facundo et al., 2020; Sunkar et al., 2023) demonstrating very competitive pricing compared to other adsorbent materials. From a chemical point of view, ACs present hydrophobic surfaces, which enhance the VOC adsorption and mitigate the competitive adsorption of water regarding hydrophilic adsorbents. ACs also possess good mechanical properties with a high resistance to compression strength, avoiding the loss of efficiency by crashing when packed in large columns.

In general, the carbonization step involves the thermal decomposition of the chemical structure of organic precursors in an atmosphere free of oxidant species. The breakage of the weaker chemical bonds generates small molecules removed as gases (CO_x, SO_x, NO_x, CH_x, H_2), pyrolysis liquids (sometimes used as precursors of biofuels) and a solid residue enriched in carbon (char), but still having a scarce porosity. The use of hydrothermal carbonization (HTC) processes allows to low the carbonization temperature by contacting raw feedstock with pressurized water, saving energy and increasing the char yield, although high pressure reactors are needed (Yao et al., 2023). After carbonization, physical or chemical activation processes develop the porosity of the char. Physical activation use reagents in gas phase (air, steam, CO_2) which induces a partial gasification of the char (activation degree). These reagents oxidize the carbon surface forming oxygenated surface groups (OSGs), which are mainly unstable at the activation temperature, thus decompose and evolve as CO. The distribution of OSGs remaining on surface determines the chemical nature of the samples. ACs obtained from barley straw by activation in steam (Pallarés et al., 2018) showed FTIR bands mainly associated to the generation of a large amount of phenols (1456 and 1377 cm^{-1}) but when use CO_2 as activating agent together phenols, the formation of aldehydes or ketones (2324–1982 cm^{-1}) and carboxylic or lactones groups (1744 cm^{-1}) was favoured, denoting the influence of the activating agent on the chemical properties of ACs.

As a result of the gasification processes and the corresponding changes on surface chemistry, new porosity is developed. The activation (burn-off) degree depends for each carbon precursor on the oxidant, temperature, and time of treatment. The microporosity and surface area usually increase at low activation degrees because new micropores are formed, but with increasing this parameter the micropores are broadened, leading to mesopores and the surface values can decrease. Moreover, the micropore development is favoured in the case of CO_2, while steam favours the formation of large micro- or even, mesopores (Molina-Sabio et al., 1996).

Compared with physical activation, generally chemical activation requires lower temperatures and times of activation (saving energy) and triggers a deeper effect on the porosity development. However, these processes are more expensive because of the use of activating chemicals such as $ZnCl_2$, KOH, H_3PO_4, etc. Moreover, these reactants are corrosive, dangerous and not environmentally friendly, although some of them, such as K_2CO_3, are more sustainable. These chemicals are mixed with carbon precursors (or their char derivatives) fitting their proportions, and then, thermally treated in an inert atmosphere. Chemical reactions produce again the partial gasification of the sample, evolving gases and developing porosity. Finally, the activated mixtures need to be carefully washed to remove the rests of chemicals and inorganic impurities. Results are dependent on the nature and proportion of precursor/chemical in the mixture, temperature of treatment and residence time (Hsiao et al., 2023; Maciá-Agulló et al., 2004).

The use of agricultural wastes to obtain ACs, and their subsequent applications in the agro-food industry, allows the valorisation of these wastes and its integration into the production system through the concept of circular economy. In this work, the characteristics and performance of a series of ACs prepared by physical or chemical activation of olive stones, a very abundant residue in Mediterranean countries, are compared. These materials will be used to develop filters to be inserted in the air recirculation systems of storage and/or transport chambers for climacteric products (Scheme 1). The development of suitable materials for the ethylene adsorption/desorption offers an intriguing technical alternative to halt ripening during storage/transport (by adsorbing ethylene, and other VOCs) or induce a controlled and appropriate level of maturation (by desorbing ethylene) when the fruit is offered for sale. Correlations between the porosity and chemical surface characteristics for these ACs with ethylene adsorption performance under dynamic conditions are stablished, trying to optimize the ACs synthesis conditions to produce materials with improved and faster ethylene adsorption-desorption processes. A comparison with different types of commercial carbon materials (ACs, fibers and carbon blacks) confirms the best performance of ACs obtained from this lignocellulosic residue.

2. Experimental

2.1. Preparation of adsorbents

As mentioned above, the main aim is to develop specific and sustainable adsorbents for ethylene removal in air streams. Upon selecting olive stones (OS) as the starting material, the properties of ACs obtained by both physical and chemical activation methods were compared. The specific conditions outlined below were tailored to enable easy comparisons between the synthesis procedures. Additional parameters, such as material yield or physical form, were also considered, influencing both cost-effectiveness and potential applications.

For the conditioning of olive stones (OS) coming from the olive oil industry, the received materials without any pre-treatment were grounded and sieved to a particle size between 1 and 2 mm, treated with 10% H_2SO_4 (98%, VWR Chemicals) solution to remove organic/inorganic rests and then, thoroughly washed with distilled water. Physically ACs were prepared in a horizontal tube furnace using a two-step process. The first step involved a carbonization with N_2 flow (150 cm^3 min^{-1}) at

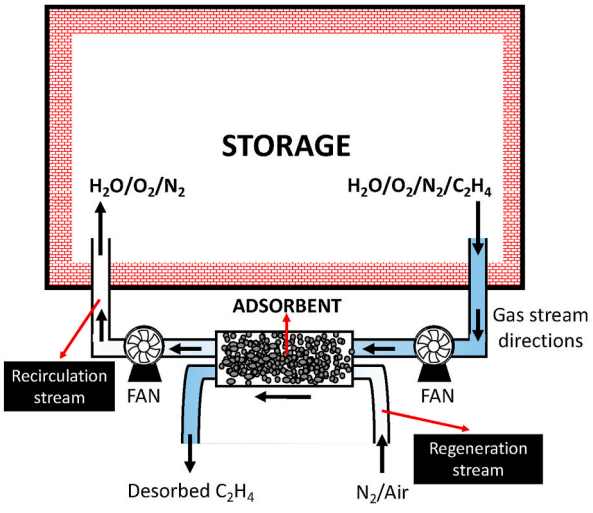

Scheme 1. Removing VOCs (ethylene) from storage chambers by adsorption/desorption using intercalated adequate filters in the air recirculation system.

10 °C min^{-1} until 800 °C with a soak time of 1.5 h. In the second step, physical activation was conducted with either CO_2 by switching the flow from pure N_2 to pure CO_2 (150 cm^3 min^{-1}) or steam. For steam activation, the N_2/steam mixture was generated by maintaining the N_2 flow used during carbonization (150 cm^3 min^{-1}) passing through a preheated glass flask at 200 °C, in which a flow of distilled water of 1.6 cm^3 min^{-1} was injected using a peristaltic pump, allowing water to be evaporated and carried away by the flow of N_2. The activating conditions were maintained during different time periods (between 3 and 4 h) to tailor the burn-off (BO) degree to the values gathered in Table 1.

Chemical activation was carried out in only one step using KOH (85%, VWR Chemicals) as activating agent. OS were directly mixed with KOH in a weight ratio of 1:2 and 1:4 and these mixtures were thermally treated for 2 h at 800 °C (10 °C min^{-1}) in N_2 flow (150 cm^3 min^{-1}) and allowed to cool down to room temperature. Samples were finally washed with diluted HCl solution and then, with distilled water until the absence of chloride ions in the washing waters was observed.

In order to compare and to study the influence of mesoporosity on the ethylene adsorption, a mesoporous carbon aerogel was also synthesized. The sol-gel process used was previously described elsewhere (Morales-Torres et al., 2010). Briefly, an aqueous solution of resorcinol (R), formaldehyde (F) and Na_2CO_3 (C) was prepared with a molar ratio of R/F = ½, R/water = 1/8, and R/C = 800, cast into glass moulds and sealed in order to prevent evaporation. The cure process involves 1 day at 30 °C, 1 day at 50 °C and 5 days at 80 °C and then, samples were cut into pellets of around 5 mm long, exchanged with acetone for 2 days, and finally, dried in supercritical CO_2. Supercritical drying is known to be the most efficient technique to preserve porous texture, and aerogels present in general wider meso-macropores and larger meso-macropore volumes than xerogels (dried by direct heat or vacuum) or cryogels (cryogenic drying) (Vivo-Vilches et al., 2015). The carbon aerogel was prepared from this organic RF-polymer by carbonization under a 100 cm^3 min^{-1} N_2 flow at 900 °C with a heating rate of 2 °C min^{-1} and soak time of 5 h (Morales-Torres et al., 2010). No activation was carried out in order to minimize the effect of microporosity and highlight the role of mesopores on the ethylene adsorption.

A complete list of all the prepared materials is gathered in Table 1, indicating the brief synthesis procedure, the activation degree of AC yield (wt.%) regarding the starting OS weight. The nomenclature used for the samples in the manuscript tries to summarize at a glance all this information. Thus, after the generic "AC" denomination, the nomenclature indicates the activating agent (K, O and S for KOH, CO_2 and steam, respectively) and the degree of activation. Thus, for instance, the ACO-24 sample refers to the AC prepared by CO_2 activation and an activation degree of 24%. Commercial carbon samples of different nature were also selected to encompass a broad range of physico-chemical properties. These commercial samples were characterized and used under the same conditions as the home-made samples. These carbons used as reference materials, include an AC in pellets (Norit® RX-3 Extra, from Norit) which will be referred as Norit in the text; a carbon black in powder form (BP2000, from CABOT) labelled as BP2000; and carbon fibers braided into fabrics (Novoloid 15–18 μm diameter, from Kynol) denoted as Kynol fabrics.

Table 1
Carbonization, activation, yield and synthesis procedure of the different carbon samples prepared by chemical or physical activation.

Sample	Synthesis	Carbonization (%)	Activation (%)	Yield (%)
ACK-92	Chemical activation (OS + KOH – 1:2)	–	92	8.0
ACK-98	Chemical activation (OS + KOH – 1:4)	–	98	2.0
ACS-13	OS carbonization + steam activation	76	13	20.9
ACS-23	OS carbonization + steam activation	76	23	18.5
ACO-14	OS carbonization + CO_2 activation	76	14	20.8
ACO-24	OS carbonization + CO_2 activation	76	24	18.2
ACO-33	OS carbonization + CO_2 activation	76	33	16.1
M900	RF polymerization + carbonization	50	–	50.0

2.2. Characterization techniques

The morphology of all carbon materials was analysed by high-resolution scanning electron microscopy (HRSEM) with a LEO (Carl Zeiss) GEMINI-1530 microscope. The textural characterization was carried out by physisorption experiments. Samples were degasified overnight at 110 °C under high vacuum (10^{-6} mbar) before determining the adsorption isotherms of N_2 at – 196 °C and CO_2 at 0 °C using a Quadrasorb SI equipment (Quantachrome, Boston Beach, FL, USA). The apparent surface area (S_{BET}) was calculated applying the Brunauer-Emmet-Teller (BET) to N_2 adsorption data at $P/P_0 < 0.10$. The micropore volume (W_0) and the mean micropore width (L_0) were obtained by applying the Dubinin-Radushkevich and Stoeckli equations, respectively (Bansal et al., 1988; Dubinin and Astakhov, 1971; Dubinin, 1989; Dubinin and Stoeckli, 1980; Stoeckli, 1981, 1990). The total pore volume (V_T) was obtained considering the volume of N_2 adsorbed at $P/P_0 = 0.95$, whilst the mesopore volume (V_{meso}) from the difference between V_T and the volume adsorbed at $P/P_0 = 0.40$ by application of Gurvich's rule (Gurvich, 1915). Quenched solid density functional theory (QSDFT) method was applied to N_2 and CO_2 isotherms to derive the pore size distribution (PSD) of samples, assuming slit-shaped pores (Neimark et al., 2009). In the absence of restriction, W_0 (N_2) yields the total micropore volume while W_0 (CO_2) estimates the narrow microporosity (micropores smaller than 0.7 nm) (Maciá-Agulló et al., 2004).

The chemical nature of samples was analysed determining the surface composition and acidity. X-ray photoelectron spectroscopy (XPS) was carried out using a Kratos Axis Ultra-DLD spectrometer. As a radiation source this instrument uses MgKα ($h\nu$ = 1486.6 eV) and a hemispherical electron analyzer operating at 12 kV and 10 mA. Survey and multi-region spectra were recorded at C1s and O1s photoelectron peaks and each spectral region was scanned several times to obtain good signal-to-noise ratios. Prior to the analysis, the samples were evacuated at high vacuum (less than 10^{-8} Torr). The point zero of charge (pH_{PZC}) of the materials was determined in degasified Milli-Q water suspensions following the method described elsewhere (Leon y Leon et al., 1992).

2.3. Ethylene adsorption performance

Dynamic adsorption experiments were performed at room temperature and atmospheric pressure using packed columns prepared in a glass reactor with an internal diameter of 0.6 cm. Preliminary experiments were conducted to optimize the column efficiency. For that, variables such as the column length, the physical properties of the backfill (particle size of ACs) and the fluid characteristics (total flow and ethylene concentration) were studied. These combinations allowed to analyse the intraparticle diffusion limitations and the influence of the contact time ($W(g_{ACs})/F(g_{ethylene}\ h^{-1})$). The experimental conditions used for the optimization of the column are summarized in Table 2.

Dimensions of the columns vary between 5 and 10 cm of length and with a total volume of 1.4 cm^3. To study the influence of particle size, physically ACs, M900 and Norit AC were milled, sieved and packed. These samples presented a similar density in such a way that the AC weight used for a column length of 10 cm was 0.5 g. However, chemically ACs or carbon black are obtained or purchased as fine powders and used without pelletization. These samples also present a smaller density, so because the volume of the column was fixed, the weight of adsorbent used decreased accordingly.

The ethylene adsorptive performance was evaluated by obtaining the

Table 2
Experimental conditions used to establish the correct performance of the columns.

Optimization factor	Experiment number	Particle size (μm)	Length (cm)	[ethylene] (mg L^{-1})	Total flow (cm^3 min^{-1})
Particle size	1	150–200	10	1000	50
	2	<150	10	1000	50
Contact time W/F	2	<150	10	1000	50
	3	<150	10	1000	25
	4	<150	10	500	50
	5	<150	5	750	50
	6	<150	5	250	50

corresponding breakthrough curves in continuous mode at atmospheric pressure. Prior to the adsorptive experiments, the adsorbent columns were pretreated at 100 °C for 1 h under N_2 flow (50 cm^3 min^{-1}) to clean the adsorbent surface before adsorption. Then, the N_2 flow was switched to an ethylene/N_2 mixture with a fitted concentration. The flow rate and concentration of ethylene in the mixture was fitted using electronic mass flow meters and controllers from Bronkhorst. The outlet gas stream was analysed by gas chromatography as a function of time in order to determine the ethylene concentration, by using a Shimadzu GC 2010 Plus chromatograph equipped with a barrier discharge ionization detector (BID) with 0.1 ppm detection limit, and a Rt-Q-BOND column (30 m, 0.53 mm ID, 20 μm).

The analysis of breakthrough curves was performed following the mass transfer zone (MTZ) concept, as described elsewhere (Zogorski and Faust, 1980). The breakthrough and saturation points are defined as the moment when the VOC concentration at the column outlet reached values of 2 and 90% of the initial VOC concentration, respectively. These values can be expressed as times on stream ($t_{0.02}$ and $t_{0.90}$) or as eluted volumes ($V_{0.02}$ and $V_{0.90}$), obtaining the amount of ethylene adsorbed at these points ($X_{0.02}$ and $X_{0.90}$) taking into account the total flow and the evolution of the ethylene concentration. The height of the mass transfer zone (H_{MTZ}) corresponds to the part of the column where adsorption is taking place, i.e., between the saturated and fresh sections of the column, thus, showing a concentration gradient between 2 and 90% of the initial concentration. The calculation of this parameter was carried out by applying the following equations (Eq 1-2):

$$H_{MTZ} = h\left(\frac{V_{0.90} - V_{0.02}}{V_{0.02} + \varphi(V_{0.90} - V_{0.02})}\right) \quad (1)$$

$$\varphi = \frac{\int_{V_{0.02}}^{V_{0.90}} (C_0 - C)dV}{C_0\,(V_{0.90} - V_{0.02})} \quad (2)$$

where h is the height of the adsorption bed and φ is the fractional capacity of the bed which is related to the efficiency of the adsorption process within the MTZ. The H_{ZTM} decreases as faster the adsorption kinetics. Because of the adsorbent is progressively saturated, the H_{MTZ} moves forward along the column with a certain rate namely, R_{MTZ} (Cheremisinoff and Ellerbusch, 1978; Mahendra et al., 2015), determined by dividing H_{MTZ} by the difference between breakthrough and saturation times, Eq (3)

$$R_{MTZ} = H_{MTZ} / (t_{0.90} - t_{0.02}) \quad (3)$$

After reaching saturation ($X_{0.90}$), the possibility for regeneration and reuse of the adsorbent was studied. Regeneration experiments were conducted without disconnecting the saturated column from the experimental setup, at room temperature, and only by replacing the ethylene/N_2 mixture flow by a similar flow (25 cm^3 min^{-1}) of pure nitrogen. The ethylene desorption processes were also monitored by gas chromatography. Consecutive adsorption-desorption cycles were performed without a loss in efficiency.

3. Results and discussion

3.1. Synthesis

The procedure of synthesis used, nomenclature and yield of samples prepared are summarized in Table 1. As commented, chemically ACs (i.e., ACK-92 and ACK-98) were obtained using one step activation procedure, avoiding the previous carbonization of OS used for physical activation. Higher activation (BO) degrees were obtained for both chemically ACs even with the lower KOH proportion. In the case of physically activated samples, the activation time was fitted to have samples with similar BO values when activated on CO_2 or steam (i.e. around 13 and 24%). The samples were prepared increasing the BO in each case by increasing the treatment time. Evidently, with increasing the activation degree decreased the AC yield. In the case of the carbon aerogel (M900), only carbonization was performed to favour the mesoporosity regarding microporosity, the yield obtained in this case being around 50.0%.

3.2. Physicochemical characterization

At a glance, it is observed that after carbonization and physical activations, ACs obtained maintain their format as grain, although the particle size is considerably reduced regarding the raw OS. However, chemically ACs are always obtained as a fine powder, indicating the stronger destruction of the OS structure. The morphology of ACO-14, ACS-23 and ACK-92 was characterized by HRSEM (Fig. 1). It is noteworthy that the adsorbent morphology is defined by the precursor and the activation method used. The analysis of the HRSEM images confirms a deeper destruction of the lignocellulosic structure after chemical activation (Fig. 1d), compared to physical activation (Fig. 1a–c). In this last case, a heterogeneous network of more defined channels and wide-open cavities derived from the original cellulosic biomaterial is shown.

N_2 and CO_2 adsorption isotherms at – 196 °C and at 0 °C, respectively, are collected in Fig. 2 and the parameters obtained from both experiments are summarized in Table 3. PSDs of selected samples were calculated applying QSDFT to the adsorption data and they are comparatively shown in Figures S1 and S2 of the supplementary material. In this table, pH_{PZC} values are also included. In general, the N_2-adsorption isotherms obtained for most ACs synthesized by physical adsorption (Fig. 2a) show a profile associated to the type I in accordance with IUPAC classification (Bansal et al., 1988), denoting the predominant microporous character of the samples. The activation in steam induces a higher N_2-adsorption capacity (total pore volume) than CO_2 activations, and the microporosity seems to be wider and more heterogeneous. This effect is even observed at low BO when the corresponding PSDs are compared (Fig. S1a), but progressively differs with increasing the activation degree (ACS-23) as denoted by a larger knee at low P/P_0. In fact, with increasing the activation degree with CO_2 (ACO-33) the adsorption capacity at low P/P_0 decreased but the slope of the isotherm increased, also denoting the progressive opening of the microporosity favouring the formation of mesopores. It is noteworthy that for chemical activation samples (Fig. 2b) and mainly for ACK-98, the shape of the isotherm significantly changes, and although tends to exhibit a type I isotherm profile, the long and smooth increase in the amount adsorbed observed in the corresponding isotherm at $P/P_0 < 0.4$ denotes a more heterogeneous microporosity in all range, while the marked hysteresis cycle also confirms the formation of mesopores. PSDs obtained for chemically ACs, as depicted in Figure S1b, corroborated that the large increase in the N_2-adsorption observed for ACK-98 (Fig. 2b) was due to a marked development of mesopores with diameters ranging between 3 and 5 nm. The N_2 isotherm corresponding to the aerogel M900 is also included in Fig. 2b for comparison, but in this case the isotherm is type IV in accordance with the expected predominant mesoporous character of this sample (Bansal et al., 1988). The carbon aerogel M900 presents a monomodal PSD around mesopores of 13.5 nm (Fig. S1c), which is a

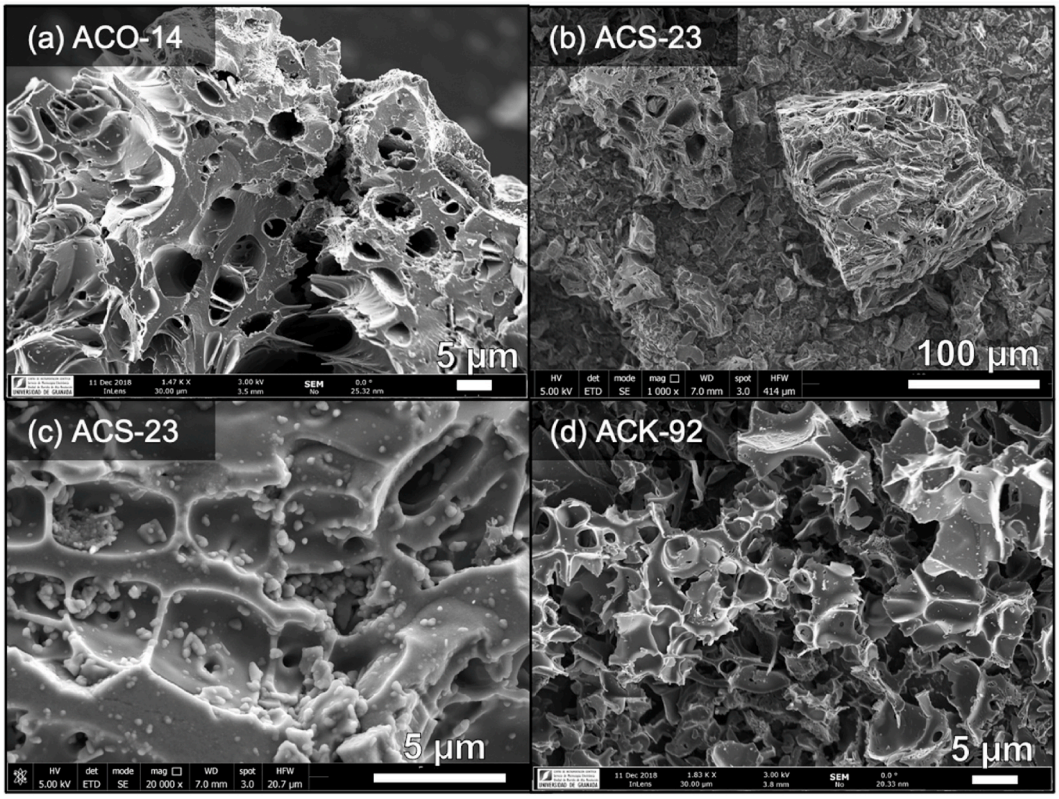

Fig. 1. HRSEM images of ACs: (a) ACO-14, (b, c) ACS-23 and (d) ACK-92.

consequence of the typical 3D structure of RF gels based on the cross-linking of homogeneous spherical nanoparticles (Morales-Torres et al., 2010). Mesoporosity corresponds to the space between particles and depends on the shrinkage along drying and carbonization procedures, while microporosity is produced inside these nanoparticles by the release of gases during carbonization. Regarding the commercial samples (Fig. 2c), the AC from Norit and the Kynol fiber are mainly microporous materials (type I isotherm), while the macro/mesoporous character of carbon black BP2000 is denoted by the isotherm profile with the progressive increase of N_2 adsorbed volume at high relative pressures ($P/P_0 > 0.9$). Thus, in this case, the corresponding PSD (Fig. S1c) progressively increased with the pore diameter, mainly for pores larger than 20 nm. This porosity is due to a more heterogeneous interparticle space.

The micropore characterization is also complemented by CO_2 adsorption experiments (Fig. 2d–f) because N_2 adsorption at – 196 °C can present certain diffusion restriction to the interior of the narrowest micropores (micropores with diameter <0.7 nm) (Leon y Leon et al., 1992; Molina-Sabio et al., 1996; Vivo-Vilches et al., 2015). As previously commented, the physical activation was carried out in two steps. The carbonization of OS produces a char (labelled as C800) with a significant BET surface area (S_{BET} = 447 m^2 g^{-1}) but scarce microporosity (W_0 = 0.19 cm^3 g^{-1}). In general, ACs present W_0 (N_2) > W_0 (CO_2), denoting the absence of diffusion restriction N_2 adsorption into the microporosity, except for the samples activated in CO_2 (Table 3). As commented, steam activation produces a greater porosity development, the values of both micropore volume (W_0) and mean micropore width (L_0) are larger than after CO_2 activation. At comparable BO (~14 wt%), the PSD of narrow micropores is monomodal after activation in CO_2 with pores of a maximum diameter around 0.6 nm, while after steam activation led to a bimodal PSD with a second maximum for pores with a dimeter of around 0.9 nm (Fig. S2a). This fact leads to that after CO_2 activation S_{mic} (CO_2) > S_{BET} (N_2), which confirms the availability of this activating agent to develop narrow micropores (Molina-Sabio et al., 1996). As consequence, ACO-14 presents the smallest micropores (L_0 = 0.57 nm) while this parameter for ACS-13 is 0.8 nm. Along the series, L_0 progressively increases with the activation degree, but for CO_2 activation even at 33% of BO the microporosity is still narrower than for the ACS-13 sample (Table 3) and still S_{mic} (CO_2) > S_{BET}, denoting that the N_2 adsorption is partially restricted by diffusion inside these narrow pores.

As commented, the largest levels of destruction of the structure and development of porosity are observed after chemical activation (Fig. 1d and 1Sb). The largest total porosity (V_T = 0.99 cm^3 g^{-1}) or BET surface area (S_{BET} = 1611 m^2 g^{-1}) were obtained after chemical activation with a ratio OS:KOH of 1:4 (ACK-98 sample). In this case, the microporosity accessible to N_2 was strongly widened L_0 = 1.75 nm, forming large micropores, which together a large volume of small mesopores (Table 3 and Fig. S1b) provokes a large contribution of non-microporous surface as denoted by the large difference between the S_{BET} and S_{mic} values. However, ACK-92 and ACK-98 present a similar PSD of narrow micropores (Fig. S2b), denoting that the strong activation process with KOH progressively opens the porosity from the external surface of the OS particle to the interior, thus generating preferentially large pores regarding the smallest ones.

All the commercial samples present similar S_{BET} values around 1300 m^2 g^{-1}, however, as commented, they present different micropore pore size and volume (Table 3). In the case of both, Norit and BP2000 samples, W_0 (N_2) > W_0 (CO_2), clearly showing the absence of diffusion restrictions. In the case of Kynol fabrics, smaller L_0 (N_2) value is observed, but W_0 (N_2) ≈ W_0 (CO_2), indicating a similar accessibility of both adsorbates and a greater homogeneity of the microporosity. In Figure S2c, the PSDs of typical mesoporous samples, i.e., BP2000 and M900, are compared. The profile observed for the BP2000 sample is also bimodal and quite similar to those obtained for ACS or ACK samples, and thus, their mean micropore width (L_0) is around 0.75 nm (Table 3), in these cases being larger than for the M900 and ACO samples.

The chemical surface properties of some representative samples were analysed by XPS to quantify the nature and concentration of oxygenated

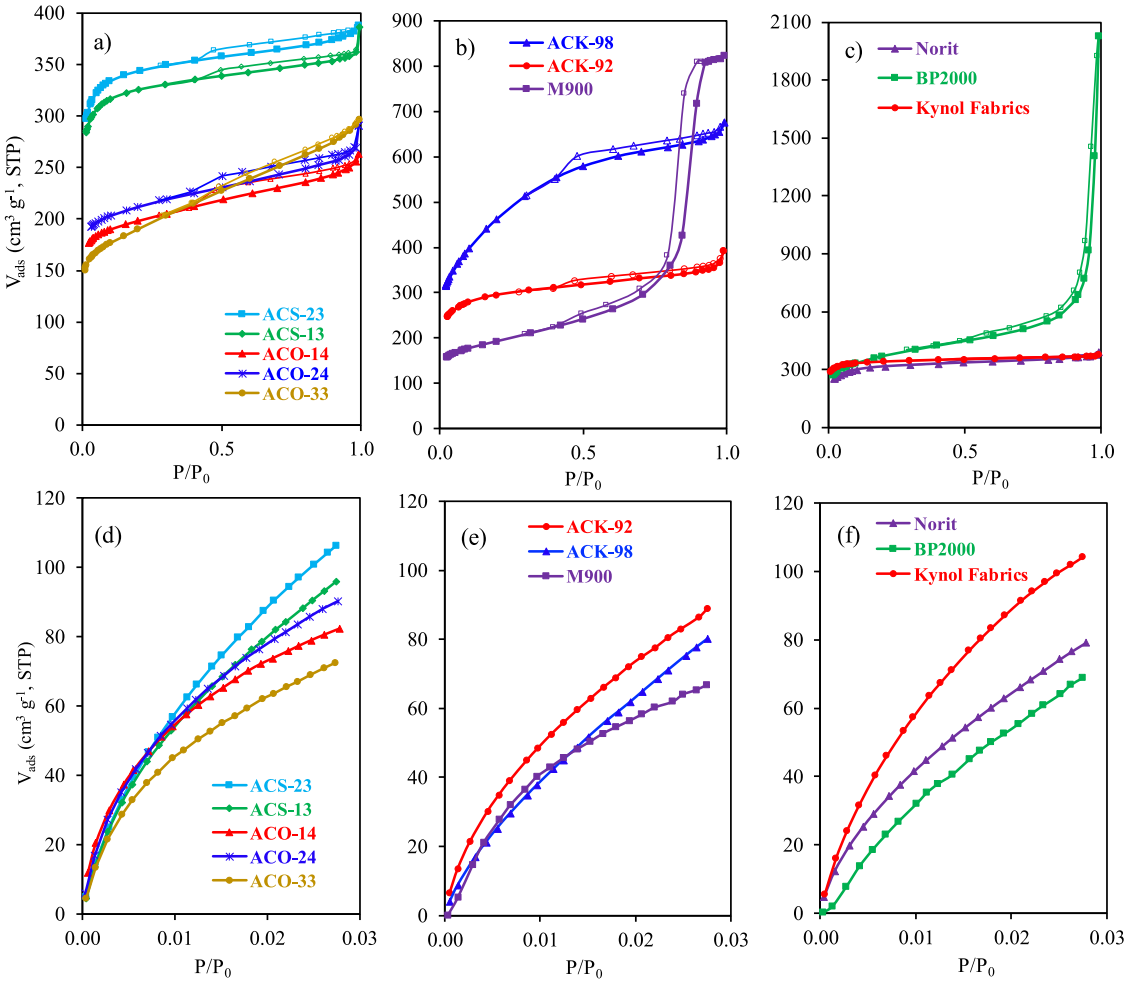

Fig. 2. N_2 adsorption-desorption isotherms (P/P_0 is the relative pressure between the equilibrium pressure and the saturation vapor pressure of N_2) (a, b, c); and CO_2 adsorption isotherms (d, e, f) for the prepared materials (a, b, d, e) and commercial carbons (c, f).

Table 3
Textural properties and pH_{PZC} of the adsorbents.

Sample	N_2 adsorption						CO_2 adsorption		
	S_{BET} (m^2 g^{-1})	W_0 (cm^3 g^{-1})	L_0 (nm)	V_{meso} (cm^3 g^{-1})	V_T (cm^3 g^{-1})	W_0 (cm^3 g^{-1})	L_0 (nm)	S_{mic} (m^2 g^{-1})	pH_{PZC}
Norit	1203	0.51	1.68	0.10	0.61	0.30	0.71	831	10.2
Kynol fabrics	1322	0.54	1.20	0.03	0.57	0.45	0.77	1169	8.0
BP2000	1342	0.56	1.67	0.54	1.20	0.29	0.79	738	7.9
ACK-92	1117	0.47	1.56	0.07	0.55	0.34	0.71	960	7.5
ACK-98	1611	0.66	1.75	0.33	0.99	0.33	0.81	828	6.1
ACS-13	1253	0.51	1.14	0.04	0.55	0.43	0.75	1157	8.8
ACS-23	1328	0.55	1.23	0.04	0.58	0.47	0.75	1267	6.7
ACO-14	745	0.27	1.07	0.06	0.39	0.29	0.57	972	10.1
ACO-24	792	0.32	1.10	0.06	0.41	0.33	0.64	1027	9.9
ACO-33	700	0.28	1.14	0.10	0.44	0.29	0.69	841	9.8
M900	702	0.29	1.44	0.90	1.26	0.24	0.61	787	8.2

S_{BET}= BET surface area; W_0 = micropore volume; L_0 = mean micropore width; S_{mic} = microporous surface area; V_{meso} = mesoporous volume; V_T = total pore volume.

surface groups (OSGs) formed during the different activation processes, which also determine the acid/basic character (pH_{PZC} values, Table 3) of the samples. The assignation of each component in the C1s and O1s spectral regions was carried out according to the literature (Figueiredo et al., 1999; Moreno-Castilla et al., 2003; Pastrana-Martínez et al., 2014). The C1s spectral region of the samples shows the presence of four components located at ≈284.6, ≈286.4, ≈287.8 and ≈ 289.8 eV assigned to aromatic/aliphatic C=C/C–C bonds, C–O (phenols, ether), C=O (carbonyl, quinone) and O–C=O bonds (carboxylic acid, anhydrides), respectively (results not shown) (Pastrana-Martínez et al., 2014). The O1s spectral region of the samples was deconvoluted into two components placed at ≈531.7 eV and ≈533.3 eV, which were assigned to C=O and C–O functionalities, respectively (Figueiredo et al., 1999; Moreno-Castilla et al., 2003; Pastrana-Martínez et al., 2014). Fig. 3a–d shows the deconvoluted high resolution XPS spectra of O1s region for the ACO-14, ACS-13, ACS-23 and ACK-98 samples, respectively. The binding energies, the corresponding peak areas, and the oxygen content (O_{XPS} %) are summarized in Table 4.

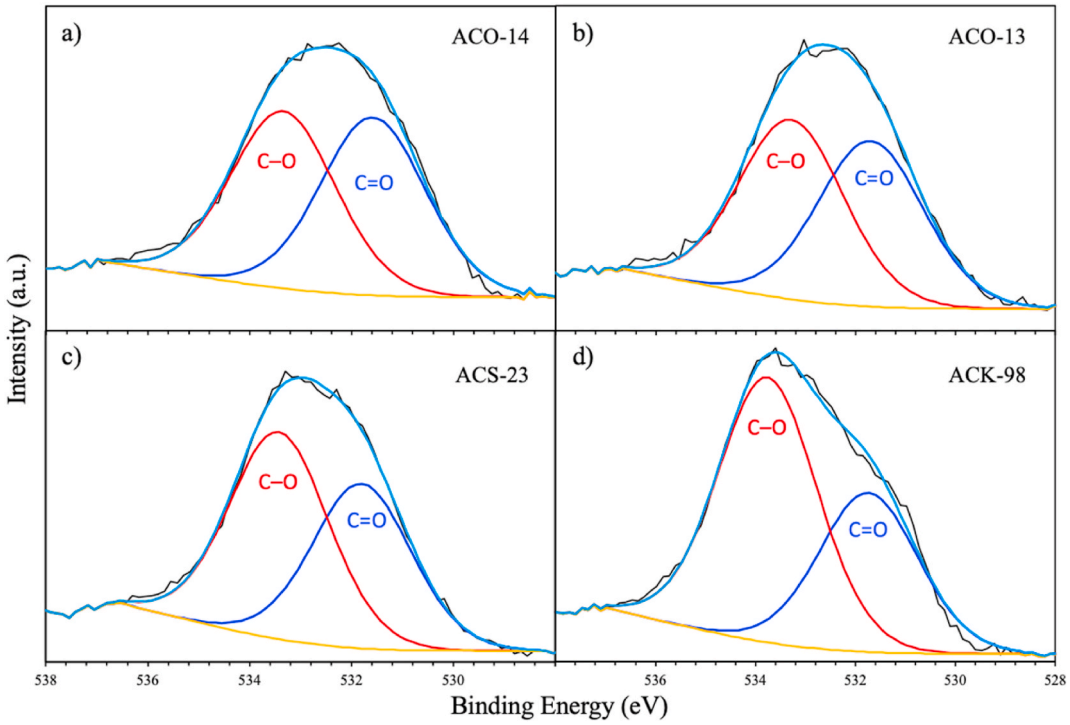

Fig. 3. O1s XPS spectral region of the different adsorbents.

Table 4
Elemental analysis of the prepared adsorbents determined by XPS (atomic content %) and distribution of carbon and oxygen species (binding energies in brackets, eV).

Sample	O_{XPS} (%)	C1s (%)				O1s (%)	
		C–C (284.6)	C–O (≈286.4)	C=O (≈287.8)	O–C=O (≈289.8)	C=O (≈531.7)	C–O (≈533.3)
Norit	5.4	43	41	10	6	57	43
ACK-98	8.7	43	39	11	7	38	62
ACS-13	5.5	45	38	11	6	48	52
ACS-23	7.1	45	37	11	7	44	56
ACO-14	5.8	49	36	10	5	50	50

The acid/basic character of the samples is related with their oxygen content and the nature of the OSGs present. The acidity (pH_{PZC}, Table 3) increases as O_{XPS} increases, both parameters being favoured with the activation degree. The C–O bonds (peak at 533.3 eV) is associated with the presence of acid groups, namely carboxylic groups. Thus, the most acidic sample corresponds to the one obtained by chemical activation under severe conditions, showing a higher oxygen content and a larger C–O proportion. A similar tendency is observed in samples activated on steam, when the activation degree increases, the pH_{PZC} decreases by the increase of O_{XPS} and C–O ratio. Comparing with the activation in CO_2, the oxygen content is comparable at similar activation degree, but the OSG distribution changes, CO_2 favouring the formation of more basic groups (ketones), thus inducing larger pH_{PZC} values. The commercial sample from Norit used as reference shows similar characteristics than ACO-14, the basic character associated to a low oxygen content with a high ratio of C=O/C–O groups.

3.3. Ethylene adsorption performance

As outlined in the experimental section (Table 2), preliminary experiments were carried out to analyse different variables influencing on the column performance. After selecting the reactor shape and dimensions, the main consideration was to optimize the conditions for both the adsorbent and adsorbate. Since physically ACs maintained the format in grain after activation, while those chemically activated were obtained as fine powder, the ACS-23 sample was selected for optimizing the conditions. To analyse the influence of the particle size of ACs on the column performance (experiments 1 and 2) this sample was milled and sieved into two fractions: i) between 150 and 200 μm (used in experiment 1), and ii) below 150 μm (used in the subsequent experiments, as explained in the results below). Columns were filled up to obtain a fixed bed of 10 cm, resulting in an approximate adsorbent amount of 0.50 g, which was clearly lower for low-density CB2000 or ACK samples. The exact weight of adsorbent in each column was ultimately used to determine the adsorption capacity. Breakthrough curves obtained from column adsorption experiment with different particle size are depicted in Fig. 4a. When decreasing the particle size, the breakthrough curves are shifted to longer breakthrough and saturation times. The results (Table 5) show that the amount of treated gas or adsorbed ethylene increases (as $V_{0.02}$ or $X_{0.02}$; $V_{0.90}$ or $X_{0.90}$) and that both H_{MTZ} and R_{MTZ} values decreases, thus increasing at the same time the efficiency and durability of the column for ACS-23 < 150 μm in comparison with ACS-23 150–200 μm. Results pointed out the diffusion restriction inside the AC's particles and the faster movement of the ethylene front using large granulated ACs. Thus, the rest of experiments were carried out fixing the particle size below 150 μm. Martínez Romero et al. (2007) also indicated the best performance of granular ACs for the ethylene adsorption regarding powdered carbons or carbon fibers even under static conditions.

The influence of operating conditions on the column adsorption experiments were also evaluated by varying the length of the column between 5 and 10 cm (experiments 5 and 6), the total flow between 25

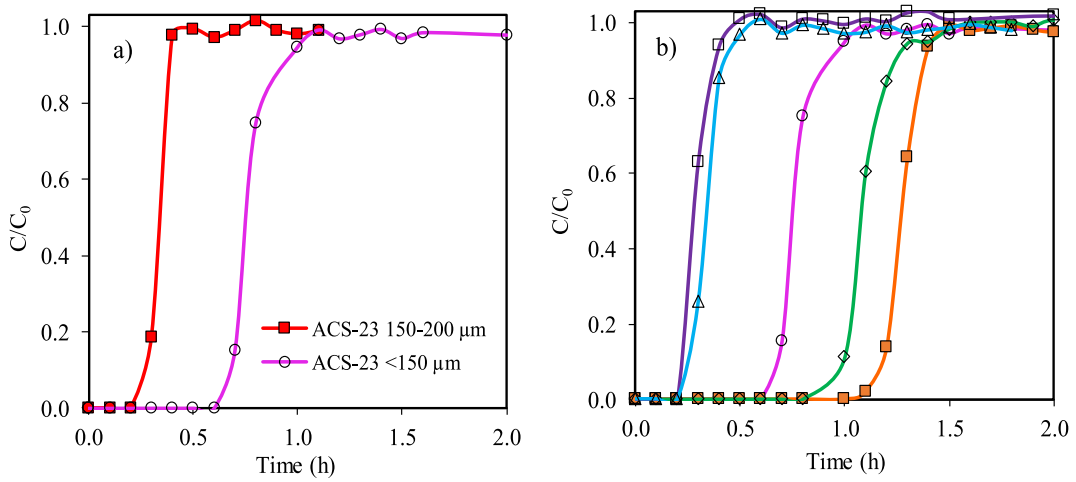

Fig. 4. Breakthrough curves of ethylene on ACS-23 at 25 °C according the conditions indicated in Table 2 a) Influence of the particle size (≤) experiment 1 (red curve), (○) experiment 2 (pink).; b) Influence of the contact time and bed depth: (□) experiment 6 (purple); (Δ): experiment 5 (blue); (○): experiment 2 (pink); (◇): experiment 4 (green); (■) experiment 3 (orange curve).

Table 5
Adsorption capacity at breakthrough and saturation points of the ACS23 sample at different experimental conditions, as stated in Table 2, and information about the movement of the ethylene front inside the columns (H_{MTZ} and R_{MTZ} values).

Experiment number	$V_{0.02}$ (L)	$V_{0.90}$ (L)	$X_{0.02}$ (μmol g^{-1})	$X_{0.90}$ (μmol g^{-1})	H_{MTZ} (cm)	R_{MTZ} (cm h^{-1})
1	0.6	1.5	55	77	2.7	8.9
2	1.8	3.0	147	177	1.8	4.4
3	1.7	2.1	134	151	1.2	4.1
4	2.4	3.9	98	128	1.3	4.5
5	0.6	1.5	80	117	1.4	4.7
6	0.6	1.4	27	32	1.1	5.6

(experiment 3) – 50 cm^3 min^{-1} and the ethylene concentrations between 250 and 1000 ppm (experiments 2–6), the obtained breakthrough curves in Fig. 4b. When columns of 10 cm length are used, the curves are shifted to higher breakthrough times halving the ethylene concentration (until 500 ppm) or the total flow (until 25 cm^3 min^{-1}). Although the contact time doubles in both cases, which should benefit the contact adsorbate/adsorbent, these variations do not affect the amount of ethylene retained. Decreasing the total flow but maintaining the ethylene concentration the curve shifted to longer times, but the volume of gas treated at the breakthrough point ($V_{0.02}$) as well the amount adsorbed ($X_{0.02}$) are maintained, H_{MTZ} and R_{MTZ} decreased, denoting the slower advance of a shorter front along the column, but this fact does not improve the performance of the column up to saturation, on the contrary, $V_{0.90}$ and $X_{0.90}$ are similar or even slowly decreased. The ethylene adsorption at breakthrough or saturation points ($X_{0.02}$ and $X_{0.9}$) strongly decreased when the ethylene concentration in the flow is halved, denoting that the smallest gradient of ethylene concentration hinders the diffusion inside the pores, decreasing the efficiency of the column. Even under static conditions (equilibrium adsorption), when the adsorption isotherms are determined, the amount of ethylene adsorbed progressively increased as the equilibrium concentration at each partial pressure (P/P_0) progressively filling different porosity ranges (Wang et al., 2021). The increasing uptake with increasing the adsorbate concentration in dynamic conditions has been observed previously in different systems (Mahendra et al., 2015). When columns of 5 cm length are used, there is not influence of the ethylene concentration on the breakthrough or saturation times, the profile of the breakthrough curves is very similar (Fig. 4b) because columns are too short regarding the R_{MTZ}. Thus, because the volume treated is similar in both cases, $X_{0.02}$ and $X_{0.9}$ decreased proportionally (1/3) when the concentration decreases from 750 to 250 ppm (Table 5).

Taking into account these results, the comparison between the different adsorbents was carried out using columns at the same bed depth (i.e., 10 cm) with a powder with particle size <150 μm, using a total flow of 50 cm^3 min^{-1} and the ethylene concentration fixed in 1000 ppm. Breakthrough curves obtained with chemically ACs, physically ACs and commercial samples are shown in Fig. 5a, b and c, respectively. Because of the high development of porosity observed for ACK-98, the performance of the mesoporous carbon aerogel was also included in Fig. 5b, in order to discuss the role of this porosity range. Results of ethylene adsorption are summarized in Table 5. The main difference between physical and chemical ACs when used to prepare the columns is the large difference in density, so the adsorbent weight using physically ACs was around 10 times greater than when using ACK-98 (Table 5). The carbon aerogel showed an average density value between both physical and chemical ACs.

It can be expected that the most porous sample (i.e. ACK-98) will present the best performance in ethylene adsorption. However, this sample showed the worst performance for the adsorption of ethylene in comparison with the other ACs (Fig. 5a and Table 5). This fact could be associated with the low volumetric density of their adsorption columns which provokes that, in spite that $X_{0.02}$ and $X_{0.9}$ values can be comparable with the rest of samples (because they are expressed in a weight basis), the gas flow could pass easily through the carbon particles and ethylene might be quickly detected in the exhaust gas, leading to a scarce durability of the column.

In fact, the performance of chemically ACs improves when the treatment was carried out in softer conditions. The ACK-92 density is higher as consequence of a minor development of the total porosity (V_T, Table 3), allowing a significant weight of adsorbent inside the column, increasing the breakthrough time and the interactions with the ethylene (lower H_{MTZ} and R_{MTZ} values, (Table 6). When the performance of chemically ACs and carbon aerogel (M900) is compared (Fig. 5a), the results show a similar profile of the breakthrough curves obtained for ACK-92 and M900. Nevertheless, because of the higher volumetric density of the M900 column, the amount of ethylene adsorbed, $X_{0.02}$ and $X_{0.90}$, is lower than for ACK-92. It is noteworthy that M900 presents the largest porosity of the tested series, showing a V_T even greater than ACK-98. Even so, M900 is eminently a mesoporous material, and despite the mesopores contributing less to ethylene adsorption compared to micropores, their effect is not negligible. In fact, the M900 column shows better performance and durability than most of the microporous samples tested, including the commercial ones. Thus, the activation of carbon

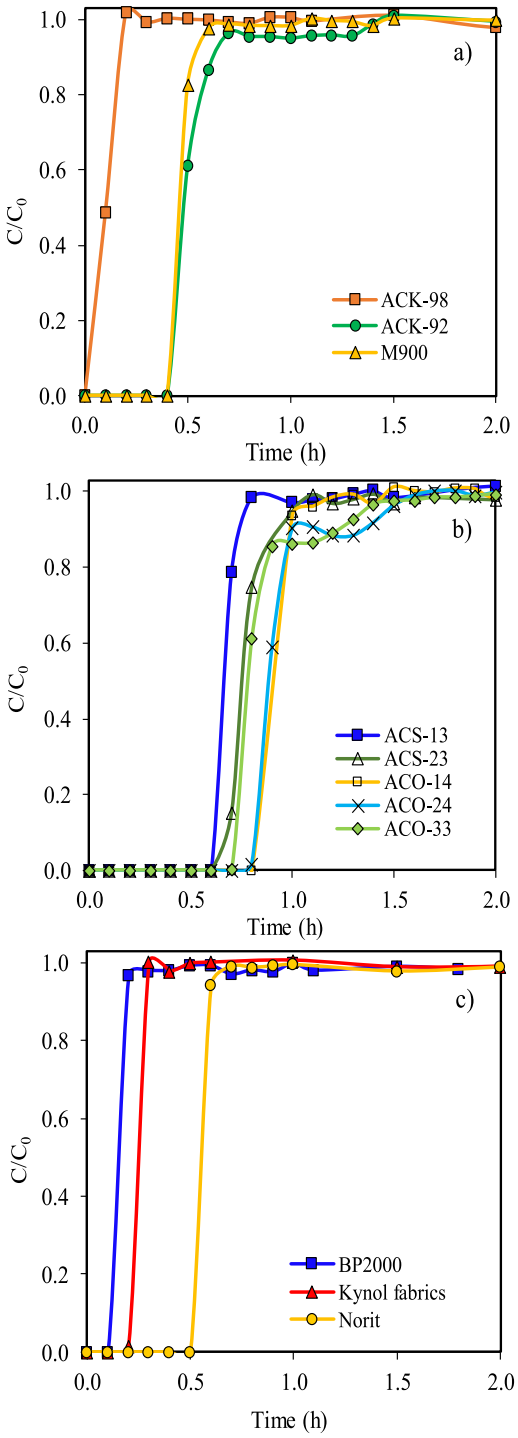

Fig. 5. Breakthrough ethylene adsorption curves on a) chemically ACs; b) physically ACs; and c) commercial carbons at 25 °C. C_0 = 1000 mg L^{-1}, total flow 50 cm^3 min^{-1} and bed depth 10 cm.

gels to produce hierarchical porosity with large meso/micropore volumes seems to be an appropriate route to prepare adsorbents for ethylene removal.

In general, the efficiency of the columns significantly improves when physically ACs are used (Fig. 5b), the best performance is observed for CO_2-activated samples. The influence of the activating agent (steam or CO_2) is clearly pointed out when comparing samples with similar activation degree (i.e. ACS-13 and ACO-14) where larger breakthrough times are observed for the samples activated in CO_2 regarding those

Table 6
Comparison between synthesized ACs and commercial samples in the ethylene adsorption. C_0 = 1000 mg L^{-1}, total flow 50 cm^3 min^{-1} and bed depth 10 cm.

Adsorbents	Weight (g)	$V_{0.02}$ (L)	$V_{0.90}$ (L)	$X_{0.02}$ (μmol g^{-1})	$X_{0.90}$ (μmol g^{-1})	H_{MTZ} (cm)	R_{MTZ} (cm h^{-1})
ACS-13	0.50	1.8	2.4	136	142	0.9	4.5
ACS-23	0.50	1.8	3.0	147	177	1.8	4.4
ACO-14	0.50	2.4	3.0	181	185	1.1	5.3
ACO-24	0.50	2.4	4.2	166	185	1.0	1.6
ACO-33	0.50	2.1	3.9	146	166	1.4	1.7
ACK-98	0.05	0.3	0.9	116	140	5.9	29.3
ACK-92	0.31	1.2	1.8	158	180	2.8	14.1
M900	0.42	1.2	1.8	117	123	1.1	5.7
BP2000	0.09	0.3	0.6	136	141	2.6	25.9
Kynol fabrics	0.20	0.6	1.2	122	123	1.2	6.2
Norit	0.54	1.5	1.8	114	115	0.9	8.8

activated on steam. When analysing the influence of the activation degree, it is observed that the adsorption performance of the samples obtained in steam improves with increasing activation (ACS-13 and ACS-23), but on the contrary, for samples activated in CO_2 the adsorption performance does not improve, and even worse, with the progressive increase in the degree of activation (Fig. 5a–Table 6). Finally, the results obtained with commercial samples (Fig. 5c) confirm some of the conclusions previously detected. The worst performance was observed for the carbon black BP2000 in spite of showing a high porosity and surface area (V_T, S_{BET} in Table 3). The use of this sample presents similar drawbacks than ACK-98, i.e., it is a very fine powder with a very low density leading to a poorly packed bed. The microporosity of kynol fabrics is quite homogeneous, without diffusional restrictions ($S_{mic} \approx S_{BET}$) and is directly accessible along the fiber axis. This sample exhibits an intermediate performance between carbon black BP2000 and granulated Norit ACs. The surface values and PSD detected (results not shown) for Norit and ACS-13 are quite similar, leading to small differences in the ethylene adsorption. Results became progressively improved from fine powder < fibers (Kynol fabrics) < granulated ACs, in agreement with those results described previously for our ACs from biomass which in general improve those results of commercial samples.

The adsorptive character described seems to be related with the physicochemical properties of the samples. Regarding the influence of the PSD, the performance described for mesoporous samples (BP2000, ACK-98 and even M900) seems to indicate that in spite of mesopores facilitates the diffusion processes, their influence on the ethylene adsorptive performance is quite limited, adsorption being more related with the evolution of the microporosity. In Fig. 6, some of the correlations observed between the parameters obtained for the dynamic ethylene adsorption and the microporous characteristics are depicted. Fig. 6a shows that the adsorption capacity ($X_{0.90}$) increased linearly with increasing the microporous surface (S_{mic} (CO_2)), but this occurs only in a certain range. However, no specific trend was observed for the surface area determined by N_2 adsorption (S_{BET}). The samples that deviate from this linearity are those obtained in steam, which perform worse than others with a lower surface area indicating the influence of additional parameters. According to Dubinin-Stoeckli equation (Bansal et al., 1988), S_{mic} increases developing W_0 and decreases with increasing L_0. The influence of the mean micropore size (L_0) on the performance of the columns is clearly observed in Fig. 6b, c and d. The breaking point ($V_{0.02}$) linearly decreases, and consequently both H_{MTZ} or R_{MTZ} increase as L_0 increases. These correlations confirm that the ethylene adsorption is mainly controlled texturally by the micropore width, being favoured on narrow micropores determined by CO_2-adsorption. This fact explains the best ethylene adsorption performance observed for CO_2-activated samples due to the development of narrower micropores (L_0) regarding the activation with steam (Table 3). When analysing the influence of

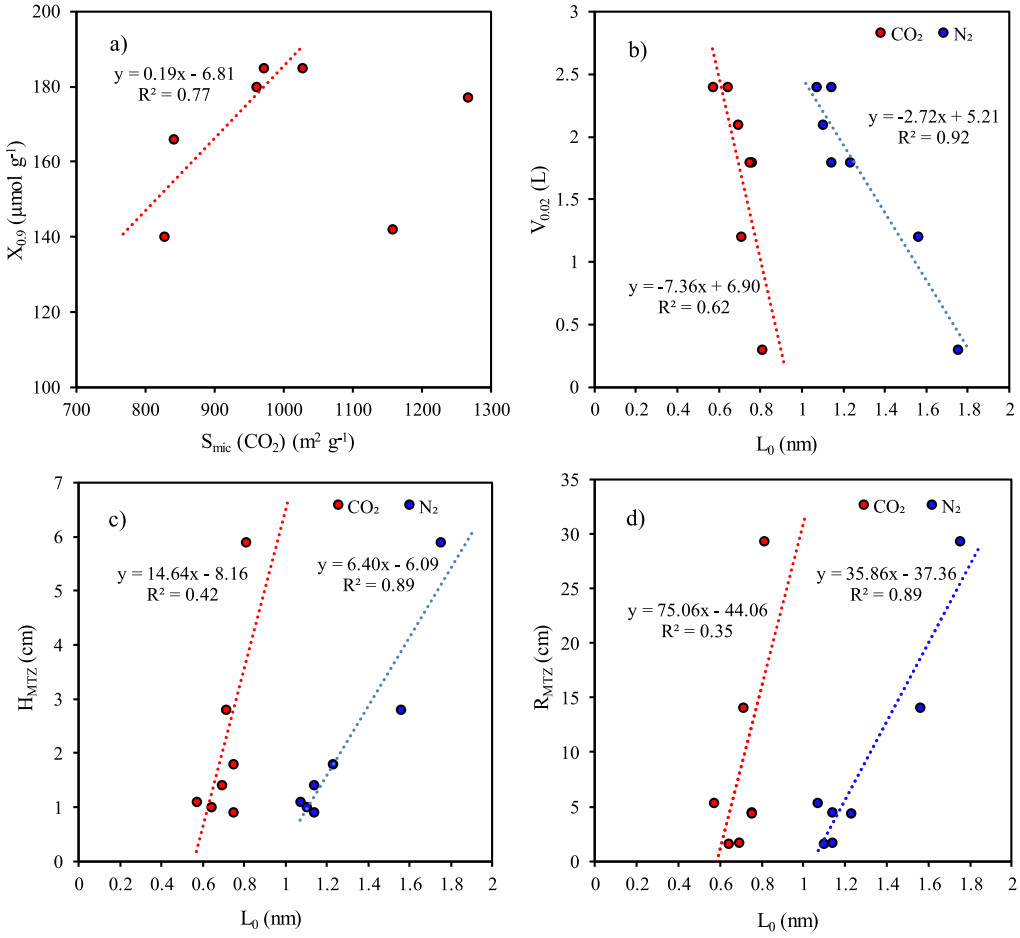

Fig. 6. Correlations between the parameters studied. $X_{0.90}$ vs S_{mic} (CO_2) and $V_{0.02}$ vs L_0 (a, b) and H_{MTZ} and R_{MTZ} vs L_0 (c, d).

increasing the activation degree from 13 to 23%, in the case of ACs obtained in steam, new micropores are created, thus increasing the micropore volume W_0 (CO_2) without enlarging the microporosity, L_0 (CO_2) is maintained (Table 3). As consequence, S_{mic} (CO_2) increased also improving in this sense the ethylene adsorption ($X_{0.02}$ and $X_{0.90}$). On the contrary, with the progressive CO_2-activation, L_0 (CO_2) progressively increased (Table 3). At intermediate activation degrees (24% BO) both W_0 and L_0 increases, leading to a compensation of effects on the ethylene adsorption capacity. Increasing the activation up to 33 wt% (ACO-33) the micropore widening led to a decrease of the microporous surface, S_{mic} (CO_2), favouring S_{BET}, which triggers to the worst ethylene adsorption performance.

All these results demonstrated that from a textural point of view the control of the narrowest microporosity is the key parameter to control the ethylene adsorption. According to previous works, the ethylene kinetic diameter is 0.416 nm (Bao et al., 2018; Saha et al., 2020) so narrow micropores enhanced the interactions with the ethylene in the flow, and both the H_{MTZ} and R_{MTZ} decreased improving the column performance (Fig. 6c and d).

These interactions are also influenced by the surface chemistry of ACs. OSGs are the most common functionalities in carbon materials, especially those prepared from lignocellulosic materials. The yield and properties of the chars depend on the balance of hemicellulose, cellulose and lignin in the precursor (Cagnon et al., 2009). When the OSG content increases, the polarity and hydrophilicity of the carbon surface increase. OSGs can be introduced in the carbon surface by oxidation treatments and progressively removed, according to their thermal stability, to fit their oxygen content and nature, and consequently, fitting the interactions with polar or non-polar VOCs. The adsorption of non-polar VOCs can be enhanced by using reductive carbonization processes (Wang et al., 2021). These processes are carried out in H_2 flow and can be assisted by Ni-nanoparticles to favour the carbon surface reduction. This treatment removes around 99.5% of the oxygen present in the cotton fiber precursors, increasing the aromaticity and hydrophobicity of the chemical structure. In addition, it strongly improves the benzene adsorption by the developed π-π interactions, but the adsorption capacity of CH_4 or C_2H_4 also enhanced with decreasing the oxygen content. The C_2H_4 adsorption capacity increased from around 1.2 to 1.3 and 1.4 mmol g^{-1} when fibers were carbonized in N_2, reductive H_2 or Ni-assisted H_2 carbonization, respectively. The introduction of nitrogen-containing functional groups into carbon materials is also used to modify the surface properties of the carbons used as a support in developing specific catalysts. Dai et al. (2019) prepared graphene/TiO_2 (GR/TiO_2) and N-doped graphene/TiO_2 (NGR/TiO_2) composites as adsorbents and/or photocatalysts for the removal of both acetaldehyde and ethylene. The results showed that N-doping favours the photodegradation of polar acetaldehyde, although an opposite effect was observed for the ethylene removal, which is related with the different interactions (adsorption) of both target molecules with the catalyst surfaces. We can conclude that increasing the functionalization of the carbon surface with heteroatoms possesses a negative effect on the interaction (adsorption) of non-polar ethylene molecules. In our case, it was detected a higher oxygen content when the activation degree increases, as well as the progressive acidification of the surface (see pH_{PZC} values in Table 3), with C–O bonds being favoured after chemical activation or physical activation on steam (determined by XPS).

The regeneration of saturated columns was also analysed, consecutive adsorption/desorption cycles were performed. All the columns were

easily regenerated; ethylene desorption was performed at room temperature only by changing the ethylene/N_2 flow by a similar pure nitrogen flow (25 cm^3 min^{-1}). Fig. 7 shows the consecutive adsorption cycles for the ACS-13 sample. Initially, the concentration of ethylene swept away for the regenerating N_2 flow is even higher than those used during the adsorption process, suggesting a weak physisorption, then progressively decreases until zero. Consecutive runs showed similar profiles denoting the reversibility of the adsorption processes. The integration of the adsorption/desorption curves allows the estimation of the amount of ethylene adsorbed at saturation point, $X_{0.90} = 124$ μmol g^{-1} while the desorbed amount was 127 μmol g^{-1}, confirming the reversibility (and reproducibility) of the process even at room temperature. Some experiments of regeneration were carried out using heating (100 °C) and/or vacuum (rotatory pump) treatments to favour a very fast regeneration (in a few minutes) but taking into account the behaviour described at room temperature, the adsorbents could be used and directly regenerated using a simple swing adsorption system with columns being adsorbing/desorbing in parallel. Our experiments corroborate the reusability of materials.

To the best of our knowledge, although several studies in the literature reporting the ethylene adsorption, references where carbon materials are used as filters for continuous ethylene adsorption is still limited. In general, the ethylene adsorption behaviour is studied under equilibrium conditions, determining the corresponding adsorption isotherms under static conditions. Mukti et al. (2018) showed that the ethylene adsorption on mesoporous ACs from waste Mangosteen rinds reached a value of 1792 μmol g^{-1} using an adsorbent with a surface area of 1080 m^2 g^{-1}. Liang et al. (2017) prepared ACs from asphalt with a surface area of 3111 m^2 g^{-1} and a pore volume of 1.92 cm^3 g^{-1}, although this sample adsorbed preferentially C_2H_6, the C_2H_4 update at $P/P_0 = 1$ was also high, leading a value between 5600 and 5900 μmol g^{-1} with an adsorption energy of 32.28 kJ mol^{-1}. Wang et al. reported the synthesis of ACs from lignosulfonate, (Wang et al., 2020) which is a by-product of the sulphite pulping process. ACs with increasing surface area were obtained by increasing the synthesis temperature up to 800 °C, leading to a maximum ethylene adsorption of 218 μmol g^{-1} at $P/P_0 = 1$. The ethylene update increased with the micropore volume by physisorption, which led to stable regeneration cycles. Miyajima et al. (2011) reported that the uptake amount of ethylene can be predicted from the micropore surface area calculated from CO_2 adsorption, which is in agreement with the influence of the narrowest porosity, as previously described in the present work.

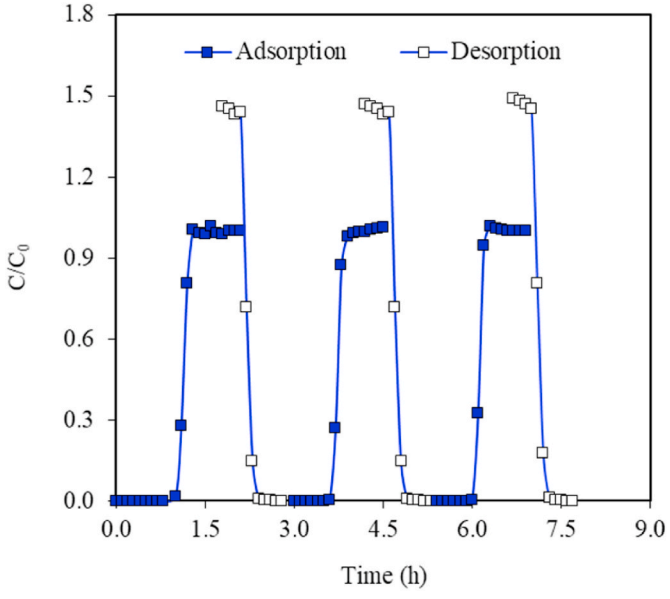

Fig. 7. Consecutive ethylene adsorption cycles for the ACS-13 sample.

However, the ethylene adsorption capacity can be enhanced with specific functionalization. Lim et al. (2020) prepared carbon aerogels functionalized with ACs and diethylenetriamine from pineapple leaf fibers that exhibit excellent ethylene adsorption capability, with a maximum adsorption of 1080 μmol g^{-1} at atmospheric pressure. On the other hand, doping with metallic phases was also used to increase the ethylene update. Cisneros et al. reported doping zeolite materials with Ag^+ species as the responsible active sites for ethylene adsorption, while selectivity is determined by the π - π complexation (Cisneros et al., 2019). The same strategy was used for carbon nanomaterials, but in this case a sulphurization of the carbon surface was needed to stabilize the charged Ag-species (Saha et al., 2020). The equilibrium uptake of ethylene on this adsorbent was about 3400 μmol g^{-1}, resulting an adsorption capacity higher than those obtained with almost all zeolite-based materials. Carbon was also doped with Cu(I) (Saha et al., 2021) or Pd(0) species (Tepamatr, 2023) which also present the complexation capacity with ethylene, thus increasing the adsorption capacity. Mesoporous RF-carbon gels doped with Cu (I) species showed a total ethylene update close to 2000 μmol g^{-1}, even higher than Cu-MOFs, such as Cu1@UiO-66-COOH and Cu1@UiO-66-$(COOH)_2$ (Zhang et al., 2020). It is necessary to mention, that in spite the π - π complexation of metallic nanoparticles with the ethylene is a reversible process, the strength of this interaction is greater than if only physisorption occurs, thus consuming also greater amount of energy during the regeneration of spent adsorbents limiting the sustainability of the process.

In spite of the difficulty to establish an adequate comparison due to the lack of results in literature obtained under similar experimental conditions, we can determine that the adsorption capacity for the different series of ethylene adsorbents previously shown by extrapolating the published isotherms at a concentration of 1000 ppm, even if these data should be higher because they are obtained in static (equilibrium). The adsorption capacity obtained with ACs from OS ranges from 150 to 180 μmol g^{-1} at room temperature, with a maximum concentration of ethylene of 1000 ppm (0.1%) in a flow system. These values are superior to those calculated for the best un-doped carbon material reported in literature (Liang et al., 2017) or even in the range of those observed for Cu-doped aerogels (Saha et al., 2021). Overall, it can be concluded that adsorbents prepared in this work are quite competitive for ethylene adsorption under dynamic conditions, showing an appropriate adsorption performance and a perfect regeneration even at room temperature.

4. Conclusions

ACs were prepared using an abundant residue from the agro-food industry such as olive stones. Three activation procedures were applied, i.e., chemical activation with KOH and physical activation with steam or CO_2, by tailoring the experimental conditions in order to obtain ACs with different activation degree and with a wide range of physicochemical characteristics. Granular ACs were obtained after physical activation, while chemical activation reduced the particle size down to a fine powder due to an extensive activation degree, which triggers simultaneously a deep porous development and the generation of acid OSGs. Steam activation produced also a greater development and opening of porosity than CO_2 at similar activation degree. The formation of narrow micropores is favoured on CO_2 stream. Steam activation also induces higher oxygen contents than CO_2 and a more acidic OSG distribution. The increase of the activation degree leads to the widening of micropores and the progressive acidification of the surface.

These adsorbents were tested as filters (fixed beds) for the removal of ethylene under dynamic conditions. The stronger difficulties for a correct performance of the column were detected using samples in powder with very low density (chemically ACs or carbon blacks) in spite of their developed porosity; granulated ACs (physically ACs and that from Norit)

offered the best solution and carbon fibers (Kynol fabrics) an intermediate behaviour. Nevertheless, the influence of diffusion process strongly influences the performance of granulated ACs, decreasing the efficiency with increasing the adsorbent particle size or decreasing the concentration of ethylene in the flow. These parameters led to higher H_{MTZ} and R_{MTZ}, i.e., a faster displacement of ethylene through the column. The amount of ethylene retained also depends on the porosity and surface chemistry of the samples, interactions with the AC surface are stronger in samples with narrow porosity and scarce oxygen functionalization. Even in these cases, the ethylene adsorption is weak (only physisorption occurs), the ethylene desorption processes take place even at room temperature, reaching the complete regeneration and allowing the reuse of the columns. With increasing the activation degree, the progressive widening of micropore and the increasing content of OSGs reduced the efficiency of the columns. Granulated adsorbents obtained by CO_2 activation with moderate activation degree showed the best performance, associated to a developed but narrow microporosity together a scarce development of OSGs. These results clearly surpass those obtained with commercial samples of different morphology and nature (carbon black, fibers or ACs) and suggest the potential suitability of these materials for use use as filters in ethylene adsorption of climacteric fruit preservation.

CRediT authorship contribution statement

Ana M. Regadera-Macías: Conceptualization, Formal analysis, Investigation, Methodology, Writing – original draft. **Sergio Morales-Torres:** Conceptualization, Data curation, Resources, Supervision, Writing – review & editing. **Luisa M. Pastrana-Martínez:** Conceptualization, Data curation, Resources, Supervision, Writing – review & editing. **Francisco J. Maldonado-Hódar:** Conceptualization, Funding acquisition, Project administration, Resources, Supervision, Writing – review & editing.

Declaration of competing interest

The authors declare that they have no known competing financial interests or personal relationships that could have appeared to influence the work reported in this paper.

Data availability

Data will be made available on request.

Acknowledgements

This work was financially supported by project PCI2020-112045 from MCIN/AEI/10.13039/501100011033 and European Union Next Generation EU/PRTR, as part of the PRIMA Programme (Nano4Fresh project). S.M.-T. (RYC-2019-026634-I) is grateful to MICIN/AEI/10.13039/501100011033 and FSE "El FSE invierte en tu futuro" for his Ramon y Cajal research contract. Funding for open access charge: Universidad de Granada / CBUA.

Appendix A. Supplementary data

Supplementary data to this article can be found online at https://doi.org/10.1016/j.envres.2024.118247.

References

Altintas, C., Keskin, S., 2022. MOF adsorbents for flue gas separation: comparison of material ranking approaches. Chem. Eng. Res. Des. 179, 308–318.
Bansal, R.C., et al., 1988. Active Carbon. Marcel Dekker, New York.
Bao, Z., et al., 2018. Molecular sieving of ethane from ethylene through the molecular Cross-section size differentiation in Gallate-based metal–organic frameworks. Angew. Chem. Int. Ed. 57, 16020–16025.
Cagnon, B., et al., 2009. Contributions of hemicellulose, cellulose and lignin to the mass and the porous properties of chars and steam activated carbons from various lignocellulosic precursors. Bioresour. Technol. 100, 292–298.
Cheremisinoff, P.N., Ellerbusch, F., 1978. Carbon Adsorption Handbook. Ann Arbor Science Publishers.
Cho, K.H., et al., 2022. Separation of ethane/ethylene gas mixture by ethane-selective CAU-3-NDCA adsorbent. Microporous Mesoporous Mater. 330, 111572.
Cisneros, L., et al., 2019. Silver nanocluster in zeolites. Adsoprtion of ethylene traces for fruit preservation. Microporous Mesoporous Mater. 283, 25–30.
Coros, M., et al., 2020. Thermally reduced graphene oxide as green and easily available adsorbent for Sunset yellow decontamination. Environ. Res. 182, 109047.
Dai, X., et al., 2019. Polarity on adsorption and photocatalytic performances of N-GR/TiO_2 towards gaseous acetaldehyde and ethylene. Appl. Surf. Sci. 485, 255–265.
de Menezes, R.F., et al., 2022. Functionalized graphene-based quantum dots: promising adsorbents for CO, NO_2, SO_2, and NH_3 pollutant gases. Mater. Today Commun. 31, 103426.
Dubinin, M., Astakhov, V., 1971. Description of Adsorption Equilibria of Vapors on Zeolites over Wide Ranges of Temperature and Pressure. ACS Publications.
Dubinin, M.M., 1989. Fundamentals of the theory of adsorption in micropores of carbon adsorbents: characteristics of their adsorption properties and microporous structures. Carbon 27, 457–467.
Dubinin, M.M., Stoeckli, H.F., 1980. Homogeneous and heterogeneous micropore structures in carbonaceous adsorbents. J. Colloid Interface Sci. 75, 34–42.
Figueiredo, J.L., et al., 1999. Modification of the surface chemistry of activated carbons. Carbon 37, 1379–1389.
Gurvich, L., 1915. Cited in SJ Gregg, KSW sing, adsorption, surface area and porosity. In: J. Phys. Chem. Soc. Russ, vol. 47. Academic Press, London, pp. 49–56 p124, 1982. as.
Hamyali, H., et al., 2022. Anthracite coal-derived activated carbon as an effectiveness adsorbent for superior gas adsorption and CO_2/N_2 and CO_2/CH_4 selectivity: experimental and DFT study. J. Environ. Chem. Eng. 10, 107007.
Hsiao, C.-H., et al., 2023. Effects of physical and chemical activations on the performance of biochar applied in supercapacitors. Appl. Surf. Sci. 610, 155560.
Hsieh, S.-L., et al., 2021. CaO recovered from eggshell waste as a potential adsorbent for greenhouse gas CO_2. J. Environ. Manag. 297, 113430.
Jones, I., et al., 2021. The application of spent tyre activated carbons as low-cost environmental pollution adsorbents: a technical review. J. Clean. Prod. 312, 127566.
Keller, N., et al., 2013. Ethylene removal and fresh product storage: a challenge at the frontiers of chemistry. Toward an approach by photocatalytic oxidation. Chem. Rev. 113, 5029–5070.
Leon y Leon, C.A., et al., 1992. Evidence for the protonation of basal plane sites on carbon. Carbon 30, 797–811.
Liang, W., et al., 2017. Asphalt-derived high surface area activated porous carbons for the effective adsorption separation of ethane and ethylene. Chem. Eng. Sci. 162, 192–202.
Lim, Z.E., et al., 2020. Functionalized pineapple aerogels for ethylene gas adsorption and nickel (II) ion removal applications. J. Environ. Chem. Eng. 8, 104524.
Luján-Facundo, M.J., et al., 2020. Preparation of sewage sludge–based activated carbon for hydrogen sulphide removal. Water, Air, Soil Pollut. 231, 187.
Maciá-Agulló, J.A., et al., 2004. Activation of coal tar pitch carbon fibres: physical activation vs. chemical activation. Carbon 42, 1367–1370.
Mahendra, C., et al., 2015. Analysis and modeling of fixed bed sorption of cesium by AMP-PAN. J. Environ. Chem. Eng. 3, 1546–1554.
Malini, K., et al., 2023. Activated carbon from biomass: preparation, factors improving basicity and surface properties for enhanced CO_2 capture capacity – a review. J. CO2 Util. 67, 102318.
Martínez-Romero, D., et al., 2007. Tools to maintain postharvest fruit and vegetable quality through the inhibition of ethylene action: a review. Crit. Rev. Food Sci. Nutr. 47, 543–560.
Miyajima, N., et al., 2011. Pore structures and ethylene adsorption behavior of polysaccharide-derived carbons. Carbon 50, 737–738.
Molina-Sabio, M., et al., 1996. Effect of steam and carbon dioxide activation in the micropore size distribution of activated carbon. Carbon 34, 505–509.
Morales-Torres, S., et al., 2010. Textural and mechanical characteristics of carbon aerogels synthesized by polymerization of resorcinol and formaldehyde using alkali carbonates as basification agents. Phys. Chem. Chem. Phys. 12, 10365–10372.
Moreno-Castilla, C., et al., 2003. Influence of carbon–oxygen surface complexes on the surface acidity of tungsten oxide catalysts supported on activated carbons. Carbon 41, 1157–1167.
Mukti, N.I.F., et al., 2018. Preparation of porous carbon as ethylene adsorbent by pyrolysis of extraction waste Mangosteen rinds. MATEC Web Conf 154, 01032.
Neimark, A.V., et al., 2009. Quenched solid density functional theory and pore size analysis of micro-mesoporous carbons. Carbon 47, 1617–1628.
Pallarés, J., et al., 2018. Production and characterization of activated carbon from barley straw by physical activation with carbon dioxide and steam. Biomass Bioenergy 115, 64–73.
Pastrana-Martínez, L.M., et al., 2014. Role of oxygen functionalities on the synthesis of photocatalytically active graphene–TiO_2 composites. Appl. Catal. B Environ. 158–159, 329–340.
Plata-Gryl, M., et al., 2022. Characterization of diatomaceous earth coated with nitrated asphaltenes as superior adsorbent for removal of VOCs from gas phase in fixed bed column. Chem. Eng. J. 427, 130653.
Saha, D., et al., 2021. Synthesis of Cu(I) doped mesoporous carbon for selective capture of ethylene from reaction products of oxidative coupling of methane (OCM). Microporous Mesoporous Mater. 328, 111488.

Saha, D., et al., 2020. Separation of ethane-ethylene and propane-propylene by Ag(I) doped and sulfurized microporous carbon. Microporous Mesoporous Mater. 299, 110099.
Stoeckli, H.F., 1981. On the theoretical foundation of the Dubinin-Astakhov equation. Carbon 19, 325–326.
Stoeckli, H.F., 1990. Microporous carbons and their characterization: the present state of the art. Carbon 28, 1–6.
Sunkar, S., et al., 2023. Adsorptive removal of acid blue dye 113 using three agricultural waste biomasses: the possibility of valorization by activation and carbonization – a comparative analysis. Environ. Res. 233, 116486.
Tepamatr, P., 2023. Efficacy of a palladium-modified activated carbon in improving ethylene removal to delay the ripening of Gros Michel banana. Journal of Agriculture and Food Research 12, 100561.
Vivo-Vilches, J.F., et al., 2015. Fitting the porosity of carbon xerogel by CO_2 activation to improve the TMP/n-octane separation. Microporous Mesoporous Mater. 209, 10–17.
Wang, S.-H., et al., 2020. Developing self-activated lignosulfonate-based porous carbon material for ethylene adsorption. J. Taiwan Inst. Chem. Eng. 115, 315–320.
Wang, Y.-H., et al., 2021. Activated carbon fibers via reductive carbonization of cellulosic biomass for adsorption of nonpolar volatile organic compounds. Colloids Surf. A Physicochem. Eng. Asp. 612, 125908.
Wei, H., et al., 2021. Ethylene scavengers for the preservation of fruits and vegetables: a review. Food Chem. 337, 127750.
Wu, H.-Y., et al., 2020. Assessment of agricultural waste-derived activated carbon in multiple applications. Environ. Res. 191, 110176.
Yang, W., et al., 2021. Ion exchange resin derived magnetic activated carbon as recyclable and regenerable adsorbent for removal of mercury from flue gases. J. Energy Inst. 97, 225–232.
Yao, F., et al., 2023. Preparation of activated biochar with adjustable pore structure by hydrothermal carbonization for efficient adsorption of VOCs and its practical application prospects. J. Environ. Chem. Eng. 11, 109611.
Zhang, L., et al., 2020. Boosting ethylene/ethane separation within Copper(I)-Chelated Metal–organic frameworks through tailor-made Aperture and specific π-complexation. Adv. Sci. 7, 1901918.
Zogorski, J., Faust, S., 1980. Carbon Adsorption Handbook.